研 究 解 説

NUMERICAL FLOW ANALYSIS OF GENERIC BODY OF CAR WITH CROSS-WIND EFFECT

Warn-Gyu PARK*, Nobuyuki TAGUCHI** and Toshio KOBAYASHI***

1. Introduction

In recent years, an automobile has been considerably improved in performance, mileage, safety, comfort, and handling quality. However, the automobile tends to be aerodynamically unstable to the crosswind and gust because of the use of light materials and streamlined shape. The center of pressure to the side force tends to move forward as the body shape becomes more aerodynamically streamlined. To determine side forces and moments acting transiently on an automobile, measurements in the wind tunnel and driving tests using a cross-wind generator have been usually used, but recently numerical analysis of automobile with cross-wind effects is becoming more and more practical by the progress of numerical algorithms and computer hardware performances.

The objective of the present work is to apply the iterative time marching scheme to the incompressible turbulent flow around a generic body of the car at the five yaw angles. Since in the wind noise aspects, the accurate flow simulation of the side-view mirror is essential, the Chimera grid technique is adopted for this purpose.

2. Mathematical and Numerical Formulation

The three-dimensional unsteady incompressible Navier-Stokes equations in a general curvilinear coordinate system (τ, ξ, η, ζ) may be written in a non-dimensional form as follows:

$$\frac{\partial \hat{q}}{\partial t}+\frac{\partial}{\partial \xi}(\hat{E}-\hat{E}_v)+\frac{\partial}{\partial \eta}(\hat{F}-\hat{F}_v)+\frac{\partial}{\partial \zeta}(\hat{G}-\hat{G}_v)=0 \quad \cdots(1)$$

First of all, let us consider the momentum equation only. Since the momentum equation is a parabolic type of partial differential equation, it can be solved using a time marching scheme as follows:

$$\begin{aligned}&\frac{1}{\Delta\tau}(\bar{q}^{n+1}-\bar{q}^{n})+\delta_\xi \bar{E}^{n+1}+\delta_\eta \bar{F}^{n+1}\\ &\quad \delta_\xi \bar{G}^{n+1}=\delta_\xi \bar{E}_v^{n+1}+\delta_\eta \bar{F}_v^{n+1}+\delta_\zeta \bar{G}_v^{n+1}\end{aligned} \quad \cdots\cdots(2)$$

The barred quantities denote the column vector matrices consisted of momentum equations in ξ-, η-, and ζ-direction. The operators, δ_ξ, δ_η and δ_ζ represent spatial differences. If the Newton iteration method is applied to efficiently solve the unsteady flow problem, Eq. (2) is rewritten as follows:

$$\begin{aligned}&\frac{1}{\Delta t}(\bar{q}^{n+1,k+1}-\bar{q}^{n})+\delta_\xi \bar{E}^{n+1,k+1}+\delta_\eta \bar{F}^{n+1,k+1}\\ &+\delta_\zeta \bar{G}^{n+1,k+1}=\delta_\xi \bar{E}_v^{n+1,k+1}+\delta_\eta \bar{F}_v^{n+1,k+1}+\delta_\zeta \bar{G}_v^{n+1,k+1}\end{aligned} \quad \cdots\cdots(3)$$

Following a local linearization of $\bar{E},\bar{F},\bar{G},\bar{E}_v,\bar{F}_v$, and $\bar{G}_v$ about the 'n+1' time level and at the 'k' iteration level,

$$\left(\frac{1}{\Delta t}+\frac{\partial}{\partial \xi}A+\frac{\partial}{\partial \eta}B+\frac{\partial}{\partial \zeta}C\right)\Delta\bar{q}=\omega\bar{R}^{n+1,k} \quad \cdots\cdots(4)$$

where ω is a relaxation factor and A, B and C are the Jacobian matrices of the flux vectors $\bar{E}-\bar{E}_v$, $\bar{F}-\bar{F}_v$, and $\bar{G}-\bar{G}_v$, respectively:

$$A=\frac{\partial(\bar{E}-\bar{E}_v)}{\partial\bar{q}};\quad B=\frac{\partial(\bar{F}-\bar{F}_v)}{\partial\bar{q}};\quad C=\frac{\partial(\bar{G}-\bar{G}_v)}{\partial\bar{q}} \quad \cdots(5)$$

and $\bar{R}^{n+1,k}$ is the residual vector defined as:

$$\begin{aligned}\bar{R}^{n+1,k}=&-\frac{\bar{q}^{n+1,k}-\bar{q}^{n}}{\Delta\tau}-(\delta_\xi \bar{E}^{n+1,k}+\delta_\eta \bar{F}^{n+1,k}+\delta_\zeta \bar{G}^{n+1,k})\\ &+(\delta_\xi \bar{E}_v^{n+1,k}+\delta_\eta \bar{F}_v^{n+1,k}+\delta_\zeta \bar{G}_v^{n+1,k})\end{aligned} \quad \cdots\cdots(6)$$

Note that LHS of Eq. (4) is the same form of discretized momentum equations, Eq. (3) at 'k' iteration level and when goes to zero, the momentum equations in their discretized form are exactly satisfied at each physical time step. Then the solution is independent

* Center for Collaborative Resarch, University of Tokyo.
** Information Technology Center, The University of Tokyo
*** Institute of Industrial Science, University of Tokyo

of any approximations made in the construction of A, B and C. To capture turbulent flows at high Reynolds number flows in detail, a suitable turbulence model is essential. In the present work, the Baldwin-Lomax turbulence model was implemented.

Next, let's consider the continuity equation. In order to solve incompressible viscous flow problems efficiently, we need a relationship coupling changes in the velocity field with changes in the pressure field while satisfying the divergence-free constraint. In the present study, the Marker-and-Cell (MAC) approach[2] is used to link the iterative changes between the pressure and velocity:

$$\Delta\left(\frac{p}{J}\right) = -\beta\left[\frac{\partial}{\partial\xi}\left(\frac{U-\xi_t}{J}\right)+\frac{\partial}{\partial\eta}\left(\frac{V-\eta_t}{J}\right)+\frac{\partial}{\partial\zeta}\left(\frac{W-\zeta_t}{J}\right)\right]^{n+1,k} \quad \cdots\cdots (7)$$

where $\Delta(p/J) = (p/J)^{n+1,k+1} - (p/J)^{n+1,k}$ and β is a relaxation factor, that may even vary from node to node as in a local time concept. Again, when p goes to zero, the continuity equation is exactly satisfied at each time step, even in unsteady flows. Eq. (7) states that if a cell is accumulating mass, then the pressure value at the next iteration is increased to repel fluid away from the cell. If a cell is losing mass, then the pressure value is lowered to draw fluid. Thus the pressure field is iteratively updated along with the velocity field until the conservation of mass is satisfied. The spatial derivatives of convective flux terms are differenced with using the third order accurate upwind QUICK (Quadratic Upstream Interpolation for Convective Kinematics) scheme[3] to reduce unphysical oscillations for high Reynolds number flows, and the spatial derivatives of viscous terms are differenced using half-point central differencing. The spatial derivatives of the continuity equation is differenced with central differencing and the fourth order artificial damping term is added to the continuity equation to stabilize the present procedure. Combining Eq. (4) and Eq. (7), and applying the numerical discretization in time and space at all nodes in the flow field, a system of simultaneous equation results for the quantity $\Delta\hat{q}$equal to (Δq/J, Δu/J, Δv/J, Δw/J). This system may be formally written as:

$$[M]\{\Delta\hat{q}\} = \{R\} \quad \cdots\cdots (8)$$

Here, since the right hand side is the discretized form of the unsteady governing equations, as long as $\{\Delta\hat{q}\}$ is driven to zero, the discretized form of unsteady Navier-Stokes equations are exactly satisfied at physical time level 'n+1'. The steady state solutions are obtained as asymptotic solutions of the time marching process. Although the matrix [M] is a sparse and banded block matrix, direct inversion of this matrix requires a huge number of arithmetic operations. A common strategy is to approximate the matrix [M] by another, easily inverted matrix [N]. In this study, matrix [N] contains only the diagonal contributions of matrix [M], and Eq. (8) becomes an explicit form which is more easily tailored for efficient execution on the current generation of vector or massively parallel computer architectures than an implicit form.

3. Chimera Grid Technique

The Chimera grid method[4] is such a conceptually simple method for domain decomposition that a major grid is generated around a main body element and minor grids are also generated to resolve interesting flow features of the specific configurations, independent to the major grid. Then, the minor grids are just overlaid on the major grid without requiring the grid boundaries to join each other in any special ways. The overlap region is required to match the solutions across boundary interfaces. The tri-linear interpolation is used to interpolate the physical quantities:

$$\begin{aligned} f_P = {} & (1-\xi)(1-\eta)(1-\zeta)f_{i,j,k} + \xi(1-\eta)(1-\zeta)f_{i+1,j,k} + \\ & (1-\xi)\eta(1-\zeta)F_{i,j+1,k} + \xi\eta(1-\zeta)f_{i+1,j+1,k} + \\ & (1-\xi)(1-\eta)\zeta f_{i,j,k+1} + \xi(1-\eta)\zeta f_{i+1,j,k+1} + \\ & (1-\xi)\eta\zeta f_{i,j+1,k+1} + \xi\eta\zeta f_{i+1,j+1,k+1} \end{aligned} \quad \cdots\cdots (9)$$

where f_p is the interpolated value of physical quantities from the data of $f_{i,j,k}$,...,$f_{i+1,j+1,k+1}$, which are values at the cell vertices. The ξ, η, are ζ distances from cell vertex as shown in figure 1. In the present work, the major grid is generated for the car body and the grid for side-view mirror is independently generated and overlaid on the major grid as shown in figure 2 (d).

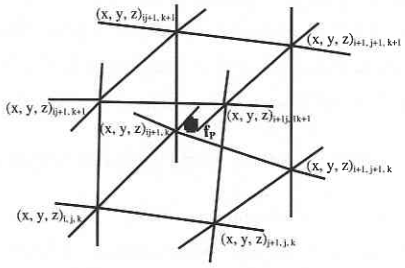

(a) Cartesian coordiante

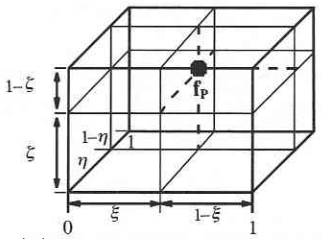

(b) Normalized local coordinate

Fig. 1 Trilinear interpolation for Chimera grid

4. Initial and Boundary Condition

It is assumed that the car is impulsively started from rest. Thus, the freestream condition is used as initial condition and farfield inflow boundary condition. At outflow boundary, $p = p_\infty$ is imposed and the velocity is extrapolated from interior nodes to account for the removal of vorticity from the flow domain by convective processes. On the body and ground surfaces, the no slip condition is applied for velocity components. The surface pressure is determined by setting the zero normal pressure gradient of pressure. For the zero yaw angle of flow simulation, the symmetry condition is applied at symmetry-plane boundary. The grid around the generic body of the car is generated using the multi-block grid technique, which is consisted of 6 blocks as shown in figure 2. The number of grid points of each blocks (Block number 1-6) are $30 \times 111 \times 67$, $78 \times 33 \times 67$, $78 \times 47 \times 32$, $78 \times 47 \times 14$, $78 \times 33 \times 67$, and $45 \times 111 \times 67$, respectively. The total number of grid points of the body is 1.1×10^6. The grid for side-view mirror is O-H grid system and grid size is $48 \times 37 \times 13$. The grid of side-view mirror is overlaid on the major grid of main body through the Chimera grid technique.

5. Results and Discussion

The present iterative time marching procedure has been applied to the flow around the generic body of the car at 1.86×10^6 of Reynolds number based on the body length. The crosswind flow is at yaw angles of 15°, 30°, 45°, and 60°. Figure 3 shows the streamlines at each yaw angles. At zero yaw angle, the A- and C-pillar vortex are evidently shown along the side end of front and rear windshield, respectively. These vortices are primarily induced by the flow separation of the sharp curves of right and left side body end and, especially, the strength of A-pillar vortex is primary wind noise source to the driver. Thus, it is important to control or reduce the A-pillar vortex strength to diminish the wind noise. The changes of flow feature as the yaw angle varies are well shown in figure 3. As the yaw angle increases, the A-and C-pillar vortex obtain their strength by the strong flow separation in the windward side-end body and these two vortices eventually coalescence togther at more than 30° yaw angle. In the leeward side, the massively flow separated region was shown. Figure 4 shows the flowfield past the side-view mirror at each yaw angles. The Chimera grid technique as mentioned before was used to simulate the flowfield around the side-view mirror. In addition to A-pillar vortex, since the flowfield around the side-view mirror also plays the significant role in the wind noise source, it is important to accurately simulate the flowfield around the side-view mirror. Figure 5 shows the limiting streamlines on the car body, as well as on the mirror surface. In this figure, S_1-S_4 denote the saddle point and N_1-N_2 denote the focal point. Figure 6 shows the streamwise surface pressure distribution along the windward, symmetry, and leeward plane. Here, the windward and leeward plane are located at a quarter width of car body from both side-ends. The numerical Cp calculation was also compared with experiment[5] in figure 6. The

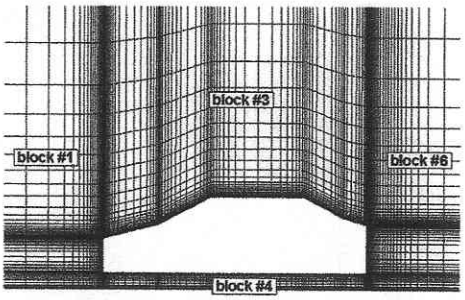

(a) Side View

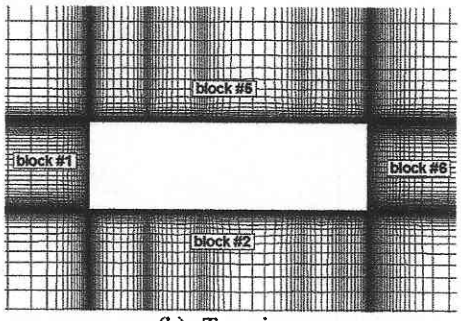

(b) Top view

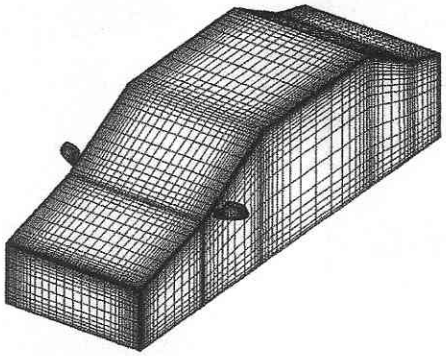
(c) Surface grid

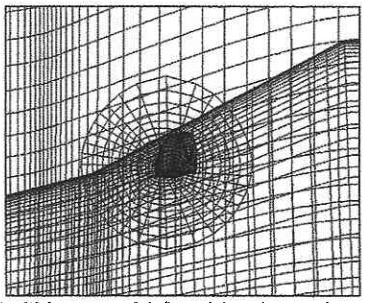
(d) Chimera grid for side-view mirror

Fig. 2 Grid system of the generic body and mirror

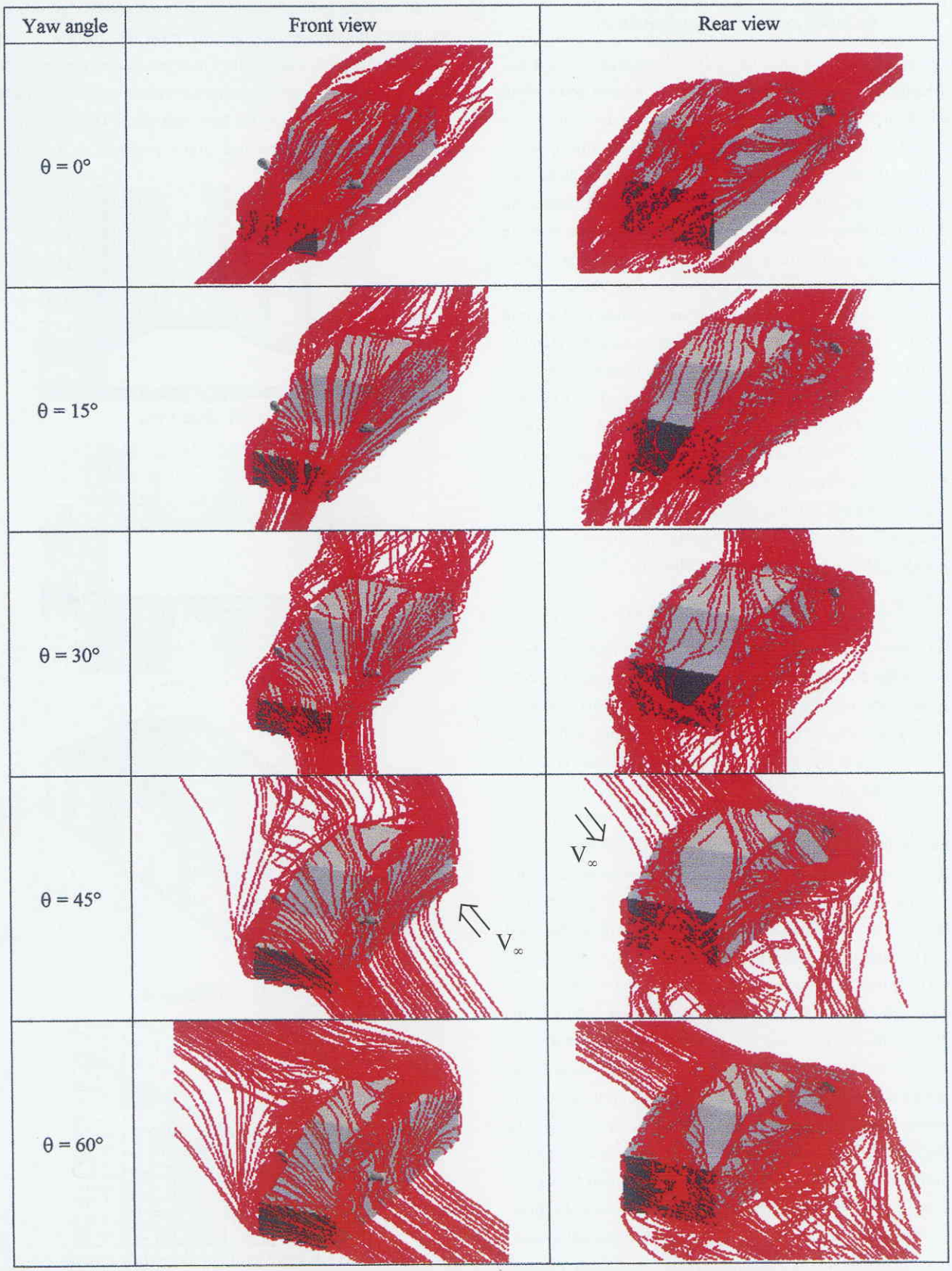

Fig. 3 Streamlines around generic body at each yaw angles

Yaw angle	Windward plane side-view mirror	Rear view plane side-view mirror
θ = 0°	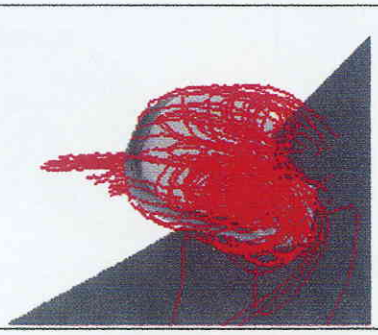	
θ = 15°	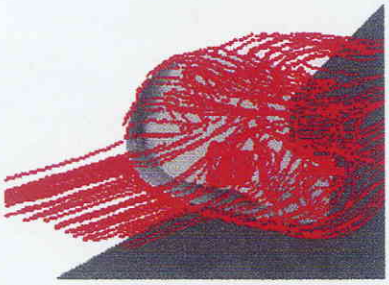	
θ = 30°	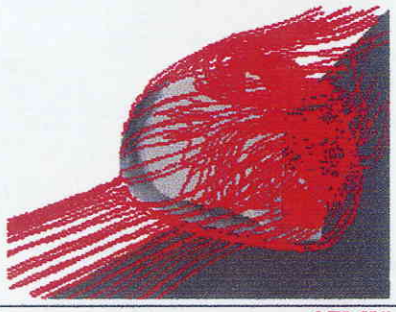	
θ = 45°	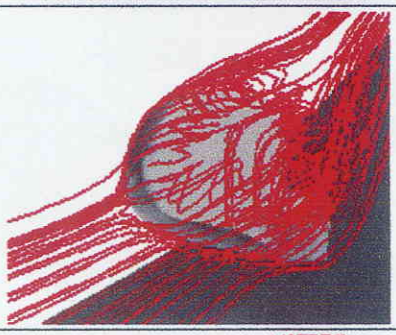	
θ = 60°	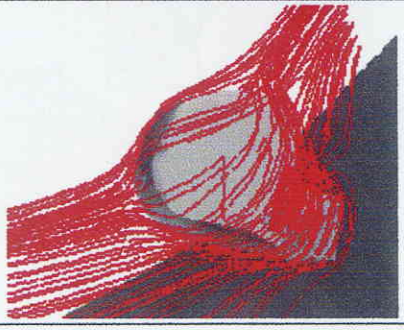	

Fig. 4 Streamlines around side-view mirror at yaw angles

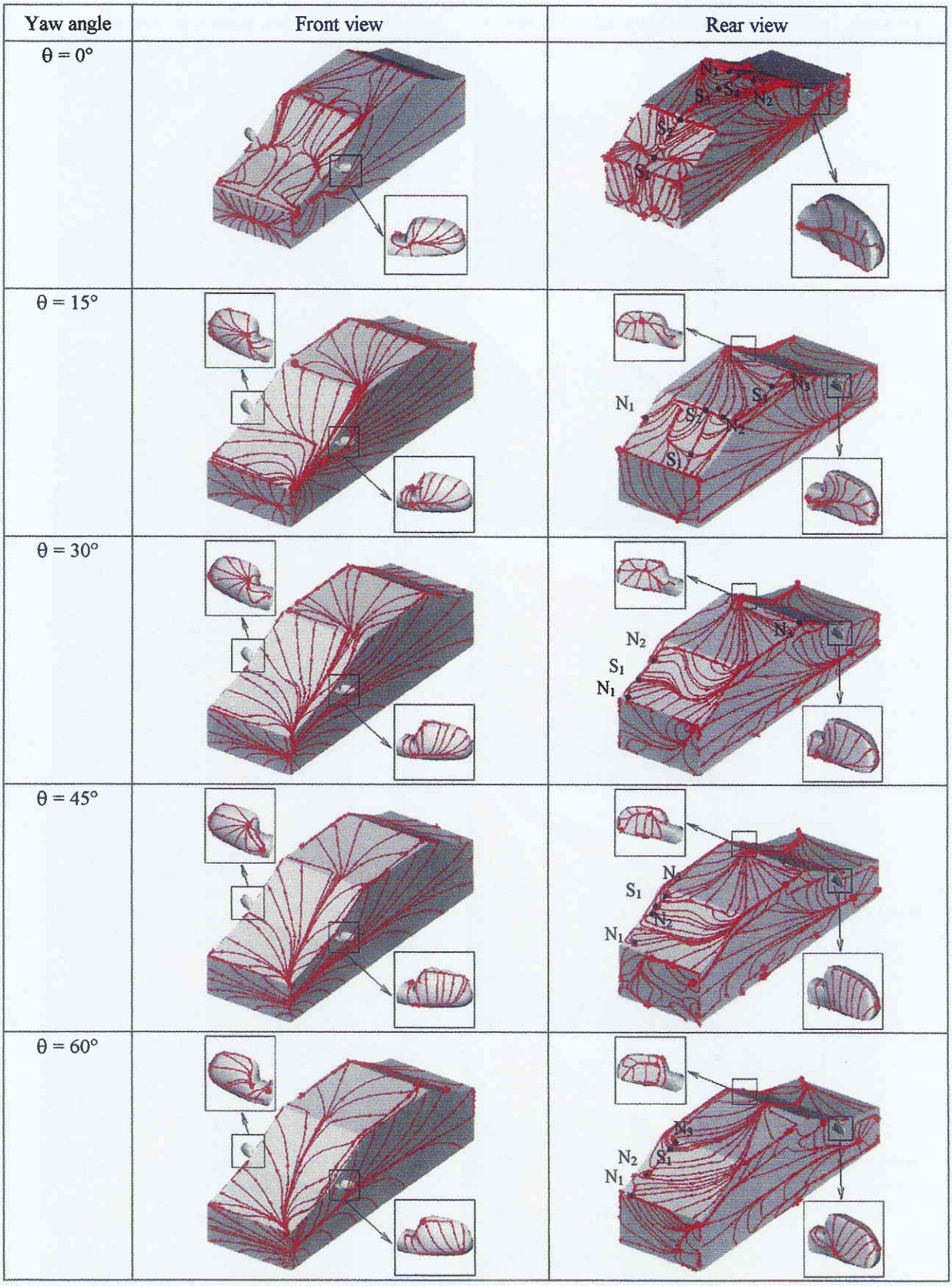

Fig. 5 Limiting streamlines on the body surface

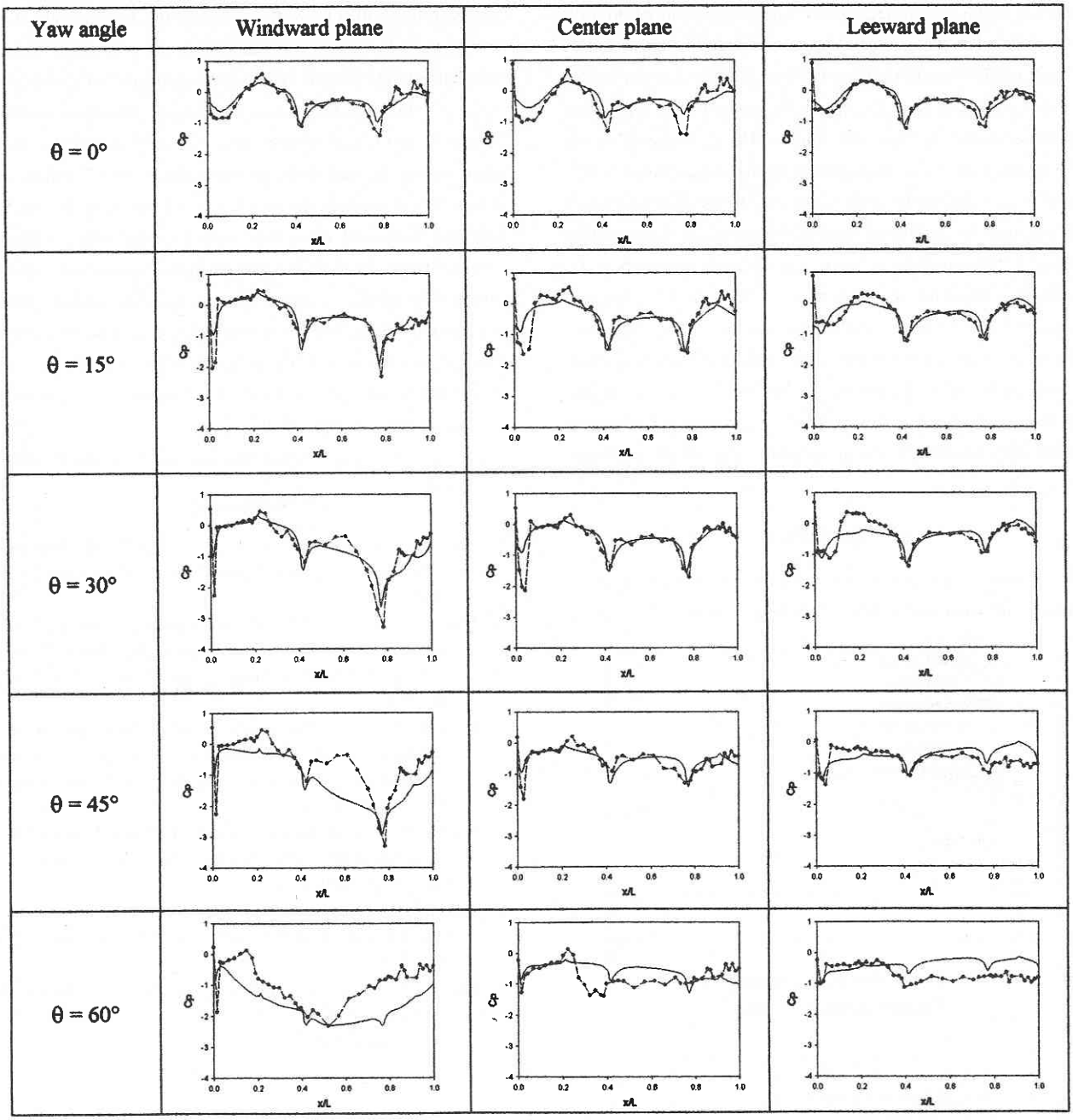

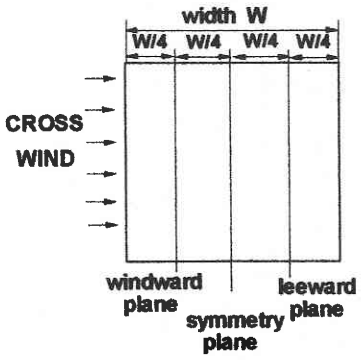

Fig. 6 Surface pressure distribution, compared with experiment[5]

numerical result agrees fairly well with experiment up to yaw angle of 30°. The discrepancies beyond 30° may be attributed to the limit of Baldwin-Lomax model. The Baldwin-Lomax model has limitations to accurately capture the massive flow separation and strong vortex at large yaw angles. The discrepancy in Cp becomes more severe in the windward plane at yaw angle of 45° and 60°, where the strong vortex generated by the flow separation is located near the designated windward plane of Cp-plot as shown in figure 3. The aerodynamic forces and moments variations as the yaw angle changes are shown in figure 7. The side force increases and lift force decreases as the yaw angle increases. The drag force is increasing up to 15° yaw angle, and, then maintains about the value of 0.6 up to 30° yaw angle. Beyond this yaw angle, the drag force is decreasing slowly. The yawing moment has same trend of drag forces. The rolling moment continuously increases very slowly.

6. Conclusions

The iterative time marching scheme for the solution of three-dimensional incompressible turbulent flows has been successfully applied to the flows around the generic body of a car having the side-view mirror under the cross-wind effect. The flow simulation has been done at zero yaw angle and four yaw angles of 15°, 30°, 45°, and 60°. From the present numerical result, the strong A- and C-pillar vortex was evidently shown at zero yaw angle and as the yaw angle increases the A- and C-pillar vortex obtain their strength by the strong flow separation in the windward side-end body and these two vortices eventually coalescence togther at more than 30° yaw angle. In the leeward side, the massively flow separated region was shown. The surface pressure distribution obtained by the present calculation was compared with experiment and agrees fairly well each other up to 30° yaw angle. The changes aerodynamic forces and moments variation are also studied as the yaw angle changes.

(Manuscript received, November 13, 2000)

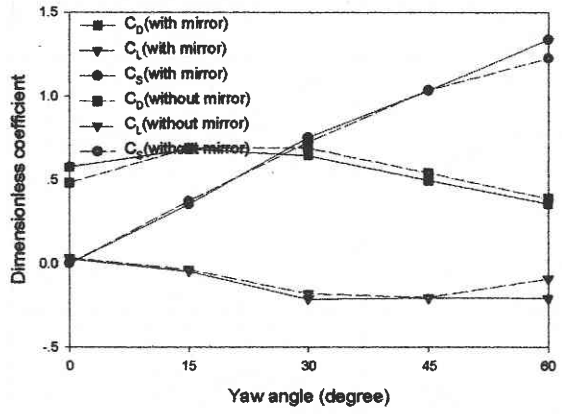

(a) aerodynamic forces

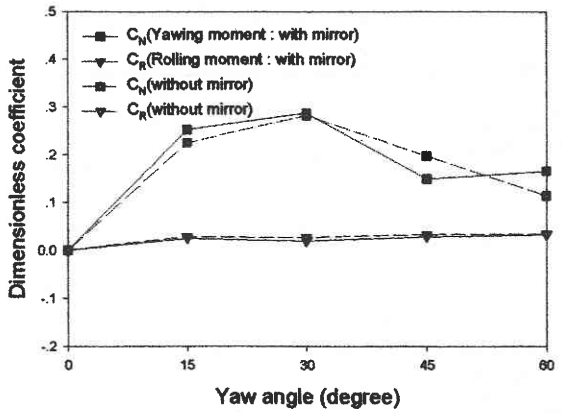

(b) aerodynamic moments

Fig. 7 Aerodynamic forces and moments variation

References

1. Park, W. G., and Sankar, L. N., "A Technique for the Prediction of Unsteady Incompressible Viscous Flows", AIAA Paper 93–3006, 1993.
2. Viecelli, J. A., "A Method for Including Arbitrary External Boundaries in the MAC Incompressible Fluid Computing Technique", Journal of Computational Physics, Vol. 4, 1969, pp. 543–551.
3. Leonard, B. P., "A Stable and Accurate Convective Modelling Procedure Based on Quadratic Upstream Interpolation", Computer Methods in Applied Mechanics and Engineering, Vol. 19, 1979, pp. 59–98.
4. Kao, K. H., Liou, M. S., and Chow, C. Y., "Grid Adaptation Using Chimera Composite Overlapping Meshes", AIAA Journal Vol. 32, No. 5, 1994, pp. 942–949.
5. Park, W. G., "Numerical Code Development for Analyzing the Flowfield and Aeroacoustic Field around an Automobile", Report of KRF, 1999.
6. Park, W. G., Jung, Y. R., and Ha, S. D., "Numerical Viscous Flow Analysis Around a High-Speed Train with Crosswind Effects", AIAA Journal, Vol. 36, No. 3, 1998, pp. 477–479.